Tuning the electronic structure of the trichloride honeycomb lattice by transition metal substitution

T. Klaproth,[1] E. Müller,[1] C. Habenicht,[1] B. Büchner,[1,2] M. Knupfer,[1] M. Roslova,[3] A. Isaeva,[1,2] T. Doert,[4] and A. Koitzsch[1,*]

[1]*Leibniz Institute for Solid State and Materials Research Dresden, Helmholtzstrasse 20, 01069 Dresden, Germany*
[2]*Institute of Solid State Physics, TU Dresden, 01062 Dresden, Germany*
[3]*Department of Materials and Environmental Chemistry, Stockholm University, Stockholm SE-10691, Sweden*
[4]*Faculty of Chemistry and Food Chemistry, TU Dresden, 01062 Dresden, Germany*

(Received 23 September 2021; accepted 18 November 2021; published 6 January 2022)

Transition metal trichlorides show peculiar and versatile magnetic properties. Whereas $CrCl_3$ is a layered antiferromagnet with potential applications as an ultrathin two-dimensional magnet, α-$RuCl_3$ may host a spin-liquid state driven by Kitaev interactions. The interest to control their material properties by chemical modifications is immense, both from an application related and from a fundamental point of view. Here, by studying $CrCl_3$, $Cr_{0.5}Ru_{0.5}Cl_3$, and α-$RuCl_3$ by photoemission and electron energy-loss spectroscopy, we find that transition metal substitution changes the optical properties of the host without compromising its underlying electronic structure. It does so by a Cr–Ru related charge transfer process across the Mott gap effectively opening up a new absorption channel below the principal gap edge of $CrCl_3$. The Cr and Ru valencies as well as the respective valence band density of states remain stable for the mixed $Cr_{0.5}Ru_{0.5}Cl_3$ compound. Our study underlines the potential of transition metal substitution as a means of material engineering of trichlorides.

DOI: 10.1103/PhysRevMaterials.6.014001

I. INTRODUCTION

Although known for a long time transition metal trichlorides have attracted intense scientific attention only recently. They do so in distinctly different contexts depending on the specific compound. For α-$RuCl_3$ signatures of spin-liquid behavior have been found, a long sought exotic state with no magnetic order triggered by Kitaev type magnetic interactions [1–3]. The actual magnetic ground state of α-$RuCl_3$ is, however, determined by a subtle interplay of Kitaev and Heisenberg interactions, resulting in antiferromagnetic order at low temperatures [4–7]. Attempts have been made to modify α-$RuCl_3$ chemically in order to change the magnetic properties. Substitution of Ir or Cr for Ru has been reported [8–10], as well as electron doping by alkali metal intercalation [11–13]. In particular, Cr doping reverses the magnetic anisotropy and induces a spin glass state [14].

$CrCl_3$, on the other hand, has emerged recently as the parent compound of an ultrathin two dimensional antiferromagnet [15–17]. The isolation of ferromagnetic monolayers such as CrI_3 and $Cr_2Ge_2Te_6$ [18,19] opens new perspectives for the field of two-dimensional (2D) materials in terms of possible magnetic, magnetoelectric, and magneto-optical applications [20,21]. Contrary to CrI_3 and $CrBr_3$, which have an out-of-plane easy axis in the ordered state, the moments in $CrCl_3$ are oriented in plane [22]. This difference is a consequence of the larger spin-orbit coupling of iodine with respect to chlorine. The in-plane spin arrangement of $CrCl_3$ is thought to arise from shape anisotropy. Control over the magnetic anisotropy via material engineering is highly desirable and has been achieved by halide mixing within the series $CrCl_{3-x}Br_x$ [23]. Moreover, it has been shown that halide mixing within the three-halide series, $CrCl_{3-x-y}Br_xI_y$, opens a path to other magnetic regimes such as magnetic frustration [24]. Alternatively, transition metal substitution has been proposed to modify magnetic parameters, e.g., by isovalent tungsten [25].

Hence the response of a given transition metal trihalide to chemical modifications in general and cation substitution in particular has become of general interest. However, the usefulness of such attempts depends on the electronic structure remaining uncompromised, i.e., no valence changes occur and no complete reorganization of the band structure. On the other hand, systematic changes of the gap value must occur, since the gap of, e.g., $CrCl_3$ and α-$RuCl_3$, differs by a large margin. Here, we probe the electronic structure of $CrCl_3$, $Cr_{0.5}Ru_{0.5}Cl_3$, and α-$RuCl_3$ in a comparative study by photoemission (PES) and electron energy-loss spectroscopy (EELS). We find that bulk $Cr_{0.5}Ru_{0.5}Cl_3$ preserves the +III oxidation state of Cr and Ru and the low energy electronic structure can be considered as a superposition of $CrCl_3$ and α-$RuCl_3$. New optical transitions related to charge transfer (CT) from Cr to Ru are observed, which might offer the possibility to create new absorption channels for photons by material engineering.

II. RESULTS AND DISCUSSION

Figure 1(a) presents the crystal structure of (Ru, Cr)Cl_3. The (Ru, Cr) sites form a honeycomb lattice where each transition metal site is octahedrally coordinated by chlorine. The octahedra are edge sharing. The layers are bound only weakly to each other by van der Waals forces. The crystals are, thus,

*a.koitzsch@ifw-dresden.de

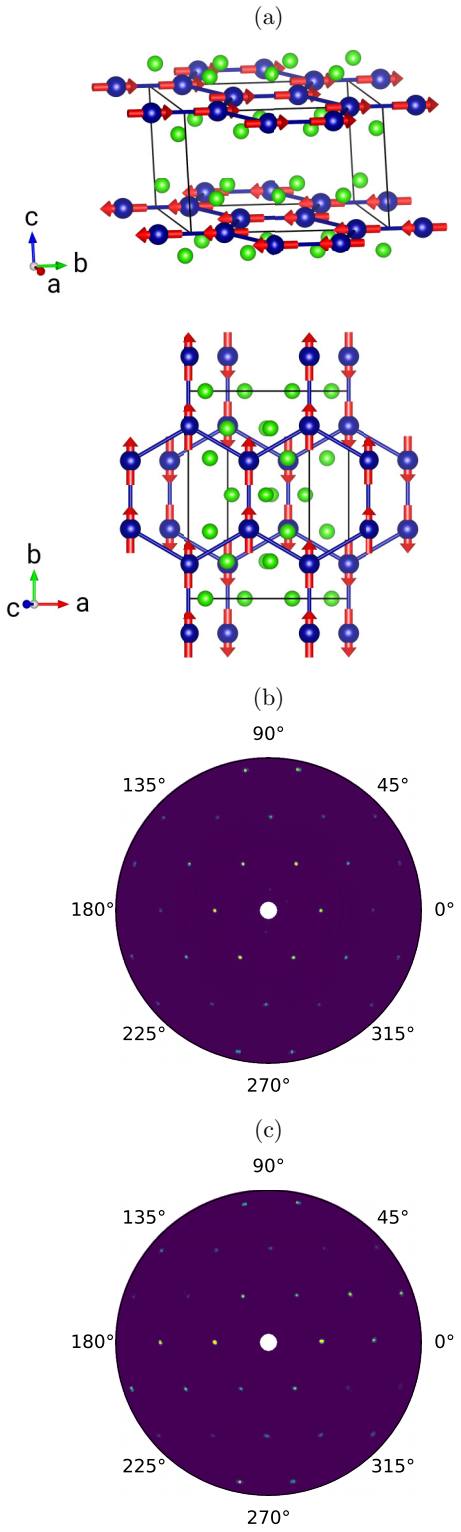

FIG. 1. (a) Crystal structure of $CrCl_3$. The red arrows represent the magnetic moments at the Cr sites. Panels (b) and (c) show zero energy-loss filtered diffraction patterns of $CrCl_3$ and $Cr_{0.5}Ru_{0.5}Cl_3$ films, respectively. The radial component corresponds to momentum transfer from 0 to 3.5 $Å^{-1}$; the bright dots are Bragg reflections demonstrating single crystalline samples.

easily cleavable. Figure 1(a) displays schematically also the magnetic structure of $CrCl_3$. The magnetic moments, arising from the $S = 3/2$ state of Cr^{3+}, are coupled ferromagnetically within each layer and oriented in plane by shape anisotropy. The individual layers are coupled antiferromagnetically along the c axis resulting in an overall antiferromagnetic ordered state below the Néel temperature $T_N = 14$ K [26,27]. Figures 1(b) and 1(c) show electron diffraction patterns for $CrCl_3$ and $Cr_{0.5}Ru_{0.5}Cl_3$. They are consistent with the honeycomb atomic arrangement in the *ab* plane of the real-space crystal structure and prove high crystallinity of the EELS samples. The distances between the diffraction spots are very similar for $CrCl_3$ and $Cr_{0.5}Ru_{0.5}Cl_3$ in agreement with the small changes in the unit cell parameters found by x-ray diffraction [9]. In addition, no superstructure is detected, which indicates that the Ru and Cr ions are randomly distributed in $Cr_{0.5}Ru_{0.5}Cl_3$. The latter conclusion is also consistent with previous diffraction results. $CrCl_3$ shows a crystallographic phase transition at $T \approx 250$ K between rhombohedral and monoclinic structures [27]. This is similar to CrI_3 and to α-$RuCl_3$, which also show such phase transitions below room temperature [28,29], leading to the question of whether or not such a structural phase transition exists also for the mixed $Cr_{0.5}Ru_{0.5}Cl_3$ crystal. The magnetic measurements on $Cr_{0.5}Ru_{0.5}Cl_3$ give no indications of a phase transition around 250 K [14]. While the transition metal substitution may significantly perturb the structural phase transition, further studies are warranted to elucidate this issue.

Cr and Ru are considered to keep their +III oxidation state in the mixed $Cr_{0.5}Ru_{0.5}Cl_3$ crystal. This has been inferred from the stable $S = 3/2$ state of Cr in $Cr_xRu_{1-x}Cl_3$ [9,14]. Figure 2(a) presents x-ray photoemission results of the Cr $2p$ core level as well as the corresponding absorption edge studied by EELS. The spectra are split by spin-orbit coupling in a $2p_{1/2}$ and a $2p_{3/2}$ component in each case. In addition, rich fine structure is observed due to multiplet splitting especially for the EELS $2p_{3/2}$ line. The agreement of the $CrCl_3$ and $Cr_{0.5}Ru_{0.5}Cl_3$ core levels explicitly confirms the purported Cr^{3+} state of the mixed compound.

We have simulated the spectral shape of XPS and EELS data using the CTM4XAS software [30] and the following parameter set for Cr^{3+} in octahedral symmetry [31]: $10Dq = 2$ eV, $\Delta = 6.5$ eV, $U = 3.3$ eV, $U_{dc} = 4.7$ eV, and $T_{e_g} = 2 \times T_{t_{2g}} = 1.7$ eV, where $10Dq$ denotes the crystal field splitting, Δ the charge transfer energy, U the on site Hubbard repulsion, U_{dc} the repulsion between the hole in the d shell and the core hole, and T_{e_g} and $T_{t_{2g}}$ the overlap integrals. The agreement is satisfactory. The splitting of the experimental XPS $2p_{3/2}$ line seen for $Cr_{0.5}Ru_{0.5}Cl_3$ is smeared out in $CrCl_3$ very likely due to photoemission related charging of this insulating compound. The latter leads also to a shift in binding energy, which has been corrected for in Fig. 2(a).

Figure 2(b) shows the Ru $3p$ lines for α-$RuCl_3$ and $Cr_{0.5}Ru_{0.5}Cl_3$. They are of very similar shape and located at equal binding energies consistent with the absence of a Ru valence change in the mixed crystal.

Figure 3(a) presents valence-band photoemission results measured with $h\nu = 40.8$ eV excitation energy (He IIα) for $RuCl_3$ and $Cr_{0.5}Ru_{0.5}Cl_3$ and $h\nu = 48.4$ eV (He IIβ) for $CrCl_3$. The latter is necessary to reduce charging effects by the approximately tenfold photon flux reduction of He II β with respect to He II α. $RuCl_3$ and $Cr_{0.5}Ru_{0.5}Cl_3$ have their first

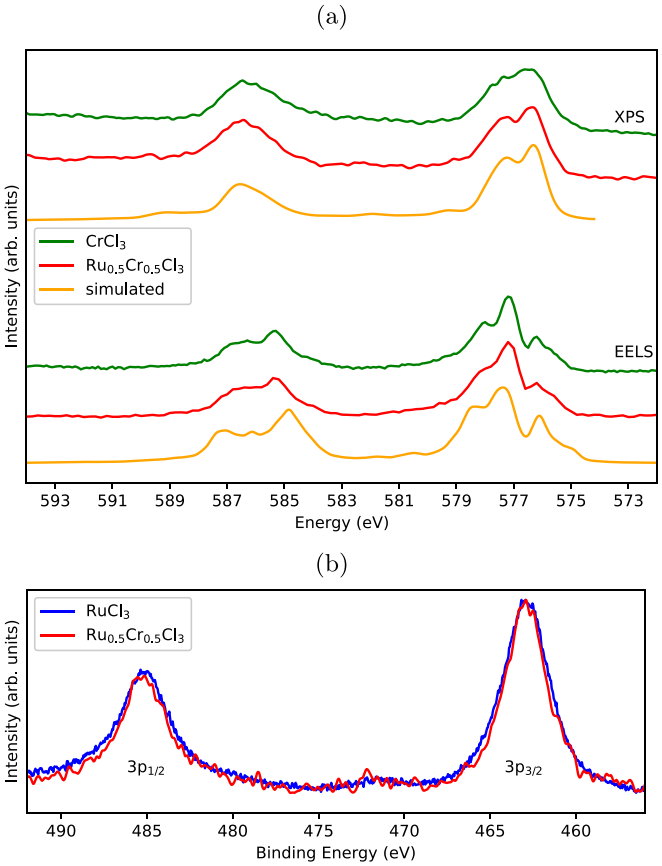

FIG. 2. (a) XPS Cr $2p$ core level spectra (upper part). Charging related energy shifts have been manually corrected in the $CrCl_3$ spectrum. EELS Cr $L_{2,3}$ edges of $CrCl_3$ and $Cr_{0.5}Ru_{0.5}Cl_3$ (lower part). The simulated spectra are obtained by the CTM4XAS package. See the text for the parameter set used. (b) XPS Ru $3p$ spectra of α-$RuCl_3$ and $Cr_{0.5}Ru_{0.5}Cl_3$.

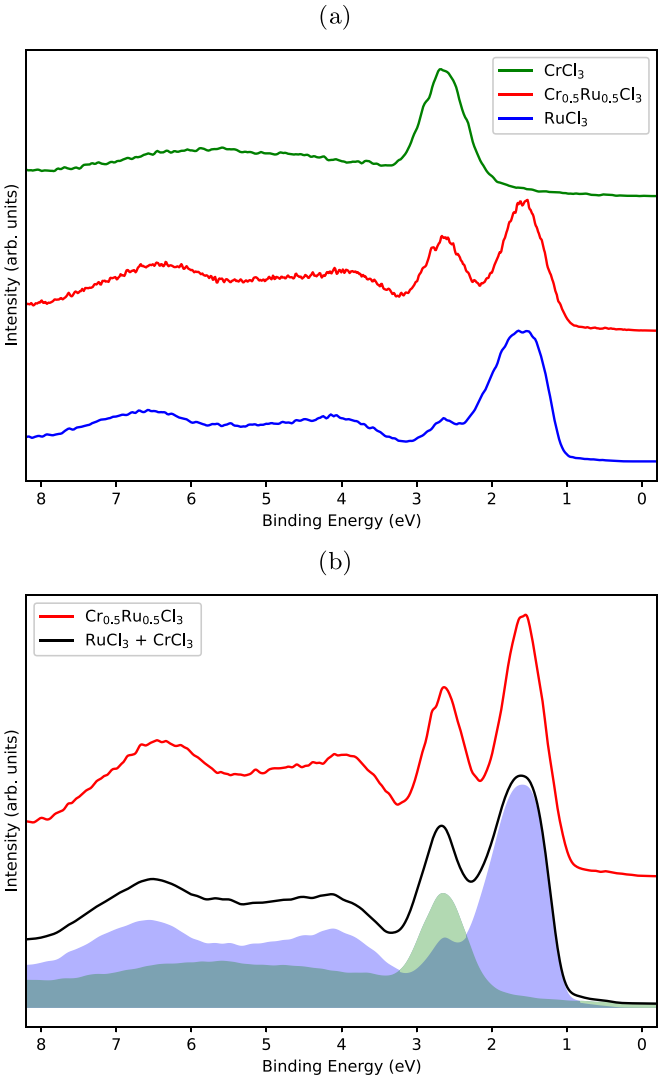

FIG. 3. (a) Valence band photoemission spectra of $CrCl_3$, $Cr_{0.5}Ru_{0.5}Cl_3$, and α-$RuCl_3$ measured with $h\nu = 40.8$ eV and $h\nu = 48.4$ eV excitation energy. Charging related shifts have been manually corrected in the $CrCl_3$ spectrum. (b) Simulation of the $Cr_{0.5}Ru_{0.5}Cl_3$ spectrum by summation of the $CrCl_3$ and α-$RuCl_3$ spectra.

peak around 1.6 eV binding energy. This peak roots in Ru $4d$ dominated density of states [32]. The peak of the pure $RuCl_3$ crystal is broader compared to the $x = 0.5$ mixed crystal. This could be a consequence of increased localization. The Cr disturbs the Ru network and reduces, thereby, the bandwidth of the Ru bands. The first and only peak of the pure $CrCl_3$ spectrum corresponds mainly to Cr $3d$ states. To correct for the charging mentioned above we have set its position manually to $E = 2.8$ eV, which is justified by earlier photoemission studies [33]. The second peak of the mixed crystal aligns to the first peak of $CrCl_3$. Figure 3(a) shows that the Cr and Ru states create rather large defect potentials of more than $\Delta E = 1$ eV with respect to each other but hardly mix.

In Fig. 3(b), the valence-band spectrum of the mixed crystals is compared to a sum of the pure spectra of $RuCl_3$ and $CrCl_3$ crystal. Except for the broadening of the first valence peak, the spectrum of the mixed crystal can be well reproduced, indicating the absence of major reorganization of the low energy electronic structure.

Electron energy-loss spectra of the three crystals at momentum transfer $\Delta q = 0.1$ Å^{-1}, which we consider to be the optical limit, are presented in Fig. 4. $CrCl_3$ shows almost no intensity up to 3.5 eV except for two weak peaks at 1.7 eV and 2.35 eV, which belong to crystal field excitations [34,35]. The intensity onset is located at $E \approx 3.2$ eV consistent with previous reports [23,34]. The orbital character of the low energy optical transitions has been assigned to strong $p - d$ excitons [36]. On the other hand, $CrCl_3$ has been classified as Mott insulator and the optical gap compares favorably with the adopted $U = 3.3$ eV (and earlier estimates of $U = 3.2$–3.7 eV) assuming small bandwidth [33]. Hence charge transfer excitations across the Mott gap should be involved at the low energy side.

The onset of excitations across the gap in α-$RuCl_3$ is, on the other hand, indicated by a prominent narrow peak at $E = 1.2$ eV followed by peaks due to singlet, crystal field, and $p - d$ excitations, which become very intense at a higher energy [37,38].

The low energy loss of the mixed crystal resembles α-$RuCl_3$. There is again the peak at $E \approx 1.2$ eV followed by

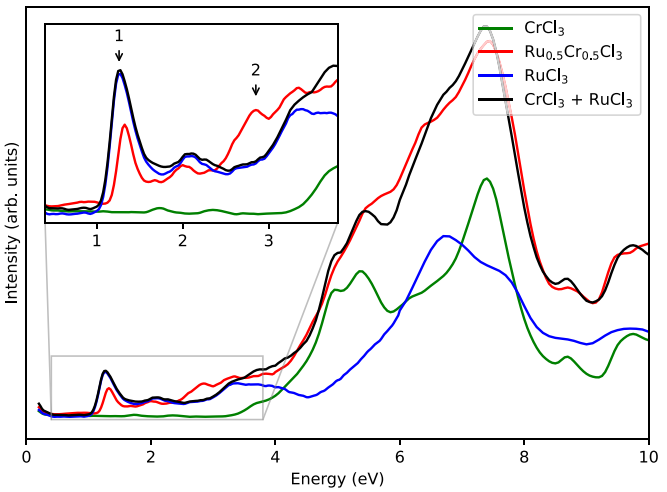

FIG. 4. Experimental EELS data in the optical limit of $CrCl_3$, $Cr_{0.5}Ru_{0.5}Cl_3$, and α-$RuCl_3$ and the sum of the spectra of $CrCl_3$ and α-$RuCl_3$. Inset: magnification of the low energy region. The locations of the main deviations of $Cr_{0.5}Ru_{0.5}Cl_3$ from $CrCl_3 + \alpha$-$RuCl_3$ are labeled "1" and "2".

smaller peaks and the strong increase above $E > 4$ eV. In fact, the spectral shape of $Cr_{0.5}Ru_{0.5}Cl_3$ at higher energies can be very well represented by a sum of the α-$RuCl_3$ and $CrCl_3$ spectra (black curve). At low energy, however, deviations occur (see inset). In particular, the principal gap excitation is reduced (labeled "1") and a new peak at $E \approx 2.8$ eV appears (labeled "2"). The reduction of peak 1 can be considered a natural consequence of the depleted ruthenium content of the sample. The origin of peak 2 is not obvious and will now be discussed in detail.

To this end Fig. 5 gives a schematic overview over the electronic structure and the low energy optical transitions of α-$RuCl_3$, $Cr_{0.5}Ru_{0.5}Cl_3$, and $CrCl_3$. The gap excitation of α-$RuCl_3$ at $E = 1.2$ eV [Fig. 5(c)] corresponds to a $d - d$ type charge transfer excitation across the Mott gap of the type $d^5 + d^5 \rightarrow d^4 + d^6$ [Figs. 5(a) and 5(b)]. The situation is similar for $CrCl_3$ but the Hubbard repulsion U and the gap value are larger. The mixed compound $Cr_{0.5}Ru_{0.5}Cl_3$ features a superposition of the gap excitations seen in α-$RuCl_3$ and $CrCl_3$. In addition, an analogous charge transfer excitation from Cr to Ru should become possible [Fig. 5(a), middle, violet arrows]. The energy of this hypothetical excitation corresponds, in a single particle description, to the difference between the Cr $3d$ dominated part of the valence band, which is inherited from $CrCl_3$, and the Ru-derived valence band [Fig. 5(b), middle].

In order to check if a Cr-Ru charge transfer excitation accounts for the additional peak at $E = 2.8$ eV in the optical response, we present in Fig. 6 a direct comparison of the photoemission and EEL spectra of $Cr_{0.5}Ru_{0.5}Cl_3$. A smooth background has been subtracted from the EELS data in the lower part. The simplest expectation from Fig. 5(b) would be that the peak separation of the $Cr_{0.5}Ru_{0.5}Cl_3$ valence band equals the peak separation of features 1 and 2. This is approximately fulfilled. The separation of the photoemission valence band peak maxima appears to be somewhat smaller than the separation of peaks 1 and 2 in the EELS spectra. Note,

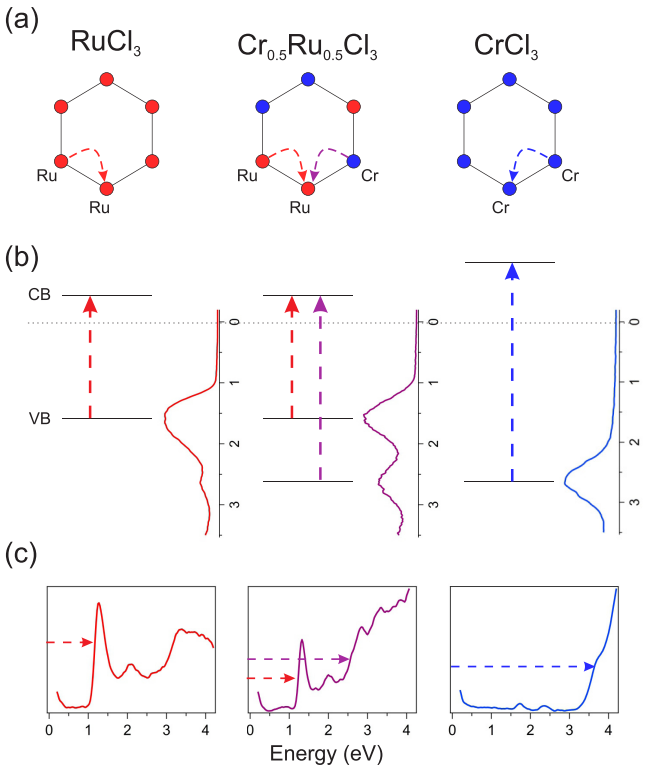

FIG. 5. Scheme of the electronic structure and optical transitions. (a) Charge transfer excitations across the Mott gap. (b) Energy levels and photoemission spectra of the valence band. (c) EEL spectra. Arrows denote optical transitions across the gap.

however, that the narrow line shape of peak 1 lies well within the valence bandwidth. So far, we adhered to a single particle description. For a more realistic comparison, excitonic many body interactions and screening have to be taken into account, which generally renormalize the spectral weight and shift transition energies to lower values. In particular, the relatively

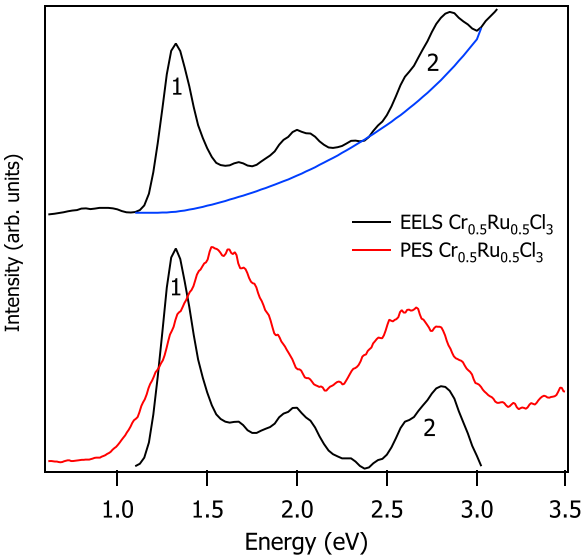

FIG. 6. Upper part: background subtraction from EELS spectrum. Lower part: comparison of EELS and photoemission data.

narrow α-$RuCl_3$ peak 1 could be affected by excitonic effects. Therefore, we consider the agreement satisfactory, which confirms the assignment of peak 2 to a Cr–Ru charge transfer transition. In principle, also the reverse CT process (Ru–Cr) should be possible.

Note that the structural phase transitions do not significantly alter the optical response in the energy range considered here [29,34,37].

Now we discuss the broader implications of our findings. An important aspect of the research on 2D magnets such as CrI_3 and $CrCl_3$ are magneto-optical coupling schemes [39]: as a means for probing the magnetic ground state but also for possible thin film applications [18,20,22,40]. The magneto-optical coupling, which is central, e.g., for measurements of the Kerr-effect or optical magnetic dichroism, generally depends on the underlying dielectric function. The photon must be absorbed in the first place in order to trigger magnetic effects. The peak at $E \approx 2.8$ eV indicates the appearance of a new absorption channel well below the principal band gap of $CrCl_3$ and, therefore, a critical modification of the dielectric function. We speculate that it could be possible to employ transition metal substitution as a means of material engineering to deliberately induce new optical absorption channels which can subsequently increase the flexibility of magneto-optical experiments by, e.g., enabling the choice of suitable laser energies as an excitation source. In the specific case of $Cr_{0.5}Ru_{0.5}Cl_3$ the high Ru content suppresses the magnetic order and induces a spin-glass state [14], which is unsuitable for the above purposes but the Ru content could be reduced or other substitution elements could be employed. We anticipate ample room for such attempts because there is a substantial number of transition metal trichlorides crystallizing in similar structures but featuring different optical absorption energies [41].

III. CONCLUSIONS

In summary, we have investigated the electronic structure of α-$RuCl_3$, $Cr_{0.5}Ru_{0.5}Cl_3$, and $CrCl_3$ by photoemission and EEL spectroscopy. The mixed compound preserves the +III oxidation states of Cr and Ru and the electronic structure resembles a superposition of its parent compounds with some localization induced band narrowing. This holds true also for the optical response except for the appearance of a new absorption channel which we assign to a Cr–Ru charge transfer. The latter strongly renormalizes the effective gap of Cr related excitations and the underlying mechanism may have some potential for tuning optical properties of chromium trihalides by transition metal substitution in general and magneto-optical processes in particular.

IV. METHODS

Crystals were grown via a chemical transport reactions technique as described in detail in Ref. [9]. All preparation steps and handling were performed in an argon-filled glovebox. For the crystal growth, pure ruthenium and/or chromium powders in stoichiometric ratios were filled into a quartz ampule together with a sealed silica capillary containing chlorine gas. After sealing off a reaction ampule under vacuum, the chlorine-containing capillary inside was broken in order to release the gas. The ampules were kept in a two-zone furnace with a temperature gradient: the range between 750 °C (source) and 650 °C (sink) for 5–8 days was used for α-$RuCl_3$ and $Cr_{0.5}Ru_{0.5}Cl_3$ crystals, while $CrCl_3$ crystals were grown between 800 °C and 700 °C for 3–6 days. All reaction products were water quenched. The homogeneity of microcrystallites' composition was confirmed by energy dispersive x-ray spectroscopy (EDX) on a Hitachi SU8020 microscope equipped with an Oxford Silicon Drift X-MaxN detector at an acceleration voltage of 10 or 20 kV and with 100 s accumulation time. The lattice symmetry and unit cell parameters were confirmed by single-crystal x-ray diffraction as described.

Photoemission spectroscopy measurements were performed using a laboratory based system equipped with a Scienta R8000 analyzer, a He discharge lamp, and an Al $K\alpha$ excitation source. The measurements have been conducted at room temperature. The intrinsic energy resolution of the valence band PES was below 20 meV and for the core levels 400 meV. Crystals have been cleaved *in situ* by the scotch tape method under a base pressure of 2×10^{-10} mbar.

The EELS measurements were carried out using a purpose built transmission electron energy-loss spectrometer with a primary electron energy of 172 keV and energy and momentum resolutions of $\Delta E = 85$ meV and $\Delta q = 0.035$ Å^{-1}, respectively, at $T = 20$ K [42,43]. The films (thickness $\approx$ 100 nm) were exfoliated using scotch tape. Subsequently, the films were mounted onto standard platinum electron microscopy grids and transferred into the EELS spectrometer.

ACKNOWLEDGMENTS

We acknowledge stimulating discussions with A. U. B. Wolter, G. Bastien, and A. Charnukha. We thank R. Hübel, S. Leger, F. Thunig, and M. Naumann for technical assistance. This work has been supported by the Deutsche Forschungsgemeinschaft (DFG) under the CRC "Correlated Magnetism—From Frustration to Topology" (SFB-1143, Project No. 247310070).

[1] K. W. Plumb, J. P. Clancy, L. J. Sandilands, V. V. Shankar, Y. F. Hu, K. S. Burch, H.-Y. Kee, and Y.-J. Kim, $\alpha - RuCl_3$: A spin-orbit assisted Mott insulator on a honeycomb lattice, Phys. Rev. B **90**, 041112(R) (2014).

[2] A. Banerjee, C. A. Bridges, J.-Q. Yan, A. A. Aczel, L. Li, M. B. Stone, G. E. Granroth, M. D. Lumsden, Y. Yiu, J. Knolle, S. Bhattacharjee, D. L. Kovrizhin, R. Moessner, D. A. Tennant, D. G. Mandrus, and S. E. Nagler, Proximate Kitaev quantum spin liquid behaviour in a honeycomb magnet, Nat. Mater. **15**, 733 (2016).

[3] C. Broholm, R. J. Cava, S. A. Kivelson, D. G. Nocera, M. R. Norman, and T. Senthil, Quantum spin liquids, Science **367**, 263 (2020).

[4] J. A. Sears, M. Songvilay, K. W. Plumb, J. P. Clancy, Y. Qiu, Y. Zhao, D. Parshall, and Y.-J. Kim, Magnetic order in $\alpha - RuCl_3$: A honeycomb-lattice quantum magnet with strong spin-orbit coupling, Phys. Rev. B **91**, 144420 (2015).

[5] R. D. Johnson, S. C. Williams, A. A. Haghighirad, J. Singleton, V. Zapf, P. Manuel, I. I. Mazin, Y. Li, H. O. Jeschke, R. Valentí, and R. Coldea, Monoclinic crystal structure of $\alpha - RuCl_3$ and the zigzag antiferromagnetic ground state, Phys. Rev. B **92**, 235119 (2015).

[6] Y. Kubota, H. Tanaka, T. Ono, Y. Narumi, and K. Kindo, Successive magnetic phase transitions in $\alpha - RuCl_3$: XY-like frustrated magnet on the honeycomb lattice, Phys. Rev. B **91**, 094422 (2015).

[7] P. Lampen-Kelley, S. Rachel, J. Reuther, J.-Q. Yan, A. Banerjee, C. A. Bridges, H. B. Cao, S. E. Nagler, and D. Mandrus, Anisotropic susceptibilities in the honeycomb Kitaev system $\alpha - RuCl_3$, Phys. Rev. B **98**, 100403(R) (2018).

[8] P. Lampen-Kelley, A. Banerjee, A. A. Aczel, H. B. Cao, M. B. Stone, C. A. Bridges, J.-Q. Yan, S. E. Nagler, and D. Mandrus, Destabilization of Magnetic Order in a Dilute Kitaev Spin Liquid Candidate, Phys. Rev. Lett. **119**, 237203 (2017).

[9] M. Roslova, J. Hunger, G. Bastien, D. Pohl, H. M. Haghighi, A. U. B. Wolter, A. Isaeva, U. Schwarz, B. Rellinghaus, K. Nielsch, B. Büchner, and T. Doert, Detuning the honeycomb of the α-$RuCl_3$ Kitaev lattice: A case of Cr^{3+} dopant, Inorg. Chem. **58**, 6659 (2019).

[10] S.-H. Do, C. H. Lee, T. Kihara, Y. S. Choi, S. Yoon, K. Kim, H. Cheong, W.-T. Chen, F. Chou, H. Nojiri, and K.-Y. Choi, Randomly Hopping Majorana Fermions in the Diluted Kitaev System α-$Ru_{0.8}Ir_{0.2}Cl_3$, Phys. Rev. Lett. **124**, 047204 (2020).

[11] X. Zhou, H. Li, J. A. Waugh, S. Parham, H.-S. Kim, J. A. Sears, A. Gomes, H.-Y. Kee, Y.-J. Kim, and D. S. Dessau, Angle-resolved photoemission study of the Kitaev candidate $\alpha - RuCl_3$, Phys. Rev. B **94**, 161106(R) (2016).

[12] A. Koitzsch, C. Habenicht, E. Müller, M. Knupfer, B. Büchner, S. Kretschmer, M. Richter, J. van den Brink, F. Börrnert, D. Nowak, A. Isaeva, and T. Doert, Nearest-neighbor Kitaev exchange blocked by charge order in electron-doped $\alpha - RuCl_3$, Phys. Rev. Materials **1**, 052001(R) (2017).

[13] Y. Imai, K. Konno, Y. Hasegawa, T. Aoyama, and K. Ohgushi, Hydrated lithium intercalation into the Kitaev spin liquid candidate material $\alpha - RuCl_3$, Phys. Rev. B **99**, 245141 (2019).

[14] G. Bastien, M. Roslova, M. H. Haghighi, K. Mehlawat, J. Hunger, A. Isaeva, T. Doert, M. Vojta, B. Büchner, and A. U. B. Wolter, Spin-glass state and reversed magnetic anisotropy induced by Cr doping in the Kitaev magnet $\alpha - RuCl_3$, Phys. Rev. B **99**, 214410 (2019).

[15] X. Cai, T. Song, N. P. Wilson, G. Clark, M. He, X. Zhang, T. Taniguchi, K. Watanabe, W. Yao, D. Xiao, M. A. McGuire, D. H. Cobden, and X. Xu, Atomically thin $CrCl_3$: An in-plane layered antiferromagnetic insulator, Nano Lett. **19**, 3993 (2019).

[16] Z. Wang, M. Gibertini, D. Dumcenco, T. Taniguchi, K. Watanabe, E. Giannini, and A. F. Morpurgo, Determining the phase diagram of atomically thin layered antiferromagnet CrCl3, Nat. Nanotechnol. **14**, 1116 (2019).

[17] D. R. Klein, D. MacNeill, Q. Song, D. T. Larson, S. Fang, M. Xu, R. A. Ribeiro, P. C. Canfield, E. Kaxiras, R. Comin, and P. Jarillo-Herrero, Enhancement of interlayer exchange in an ultrathin two-dimensional magnet, Nat. Phys. **15**, 1255 (2019).

[18] B. Huang, G. Clark, E. Navarro-Moratalla, D. R. Klein, R. Cheng, K. L. Seyler, D. Zhong, E. Schmidgall, M. A. McGuire, D. H. Cobden, W. Yao, D. Xiao, P. Jarillo-Herrero, and X. Xu, Layer-dependent ferromagnetism in a van der Waals crystal down to the monolayer limit, Nature (London) **546**, 270 (2017).

[19] C. Gong, L. Li, Z. Li, H. Ji, A. Stern, Y. Xia, T. Cao, W. Bao, C. Wang, Y. Wang, Z. Q. Qiu, R. J. Cava, S. G. Louie, J. Xia, and X. Zhang, Discovery of intrinsic ferromagnetism in two-dimensional van der Waals crystals, Nature (London) **546**, 265 (2017).

[20] B. Huang, G. Clark, D. R. Klein, D. MacNeill, E. Navarro-Moratalla, K. L. Seyler, N. Wilson, M. A. McGuire, D. H. Cobden, D. Xiao, W. Yao, P. Jarillo-Herrero, and X. Xu, Electrical control of 2d magnetism in bilayer CrI_3, Nat. Nanotechnol. **13**, 544 (2018).

[21] S. Jiang, L. Li, Z. Wang, K. F. Mak, and J. Shan, Controlling magnetism in 2d CrI_3 by electrostatic doping, Nat. Nanotechnol. **13**, 549 (2018).

[22] H. H. Kim, B. Yang, S. Li, S. Jiang, C. Jin, Z. Tao, G. Nichols, F. Sfigakis, S. Zhong, C. Li, S. Tian, D. G. Cory, G.-X. Miao, J. Shan, K. F. Mak, H. Lei, K. Sun, L. Zhao, and A. W. Tsen, Evolution of interlayer and intralayer magnetism in three atomically thin chromium trihalides, Proc. Natl. Acad. Sci. USA **116**, 11131 (2019).

[23] M. Abramchuk, S. Jaszewski, K. R. Metz, G. B. Osterhoudt, Y. Wang, K. S. Burch, and F. Tafti, Controlling magnetic and optical properties of the van der Waals crystal $CrCl_{3-x}Br_x$ via mixed halide chemistry, Adv. Mater. **30**, 1801325 (2018).

[24] T. A. Tartaglia, J. N. Tang, J. L. Lado, F. Bahrami, M. Abramchuk, G. T. McCandless, M. C. Doyle, K. S. Burch, Y. Ran, J. Y. Chan, and F. Tafti, Accessing new magnetic regimes by tuning the ligand spin-orbit coupling in van der Waals magnets, Sci. Adv. **6**, 9379 (2020).

[25] F. Xue, Y. Hou, Z. Wang, and R. Wu, Two-dimensional ferromagnetic van der Waals $CrCl_3$ monolayer with enhanced anisotropy and Curie temperature, Phys. Rev. B **100**, 224429 (2019).

[26] B. Kuhlow, Magnetic ordering in $CrCl_3$ at the phase transition, Phys. Status Solidi **72**, 161 (1982).

[27] M. A. McGuire, G. Clark, S. KC, W. M. Chance, G. E. Jellison, V. R. Cooper, X. Xu, and B. C. Sales, Magnetic behavior and spin-lattice coupling in cleavable van der Waals layered $CrCl_3$ crystals, Phys. Rev. Materials **1**, 014001 (2017).

[28] M. A. McGuire, H. Dixit, V. R. Cooper, and B. C. Sales, Coupling of crystal structure and magnetism in the layered, ferromagnetic insulator CrI_3, Chem. Mater. **27**, 612 (2015).

[29] S. Reschke, F. Mayr, S. Widmann, H.-A. K. von Nidda, V. Tsurkan, M. V. Eremin, S.-H. Do, K.-Y. Choi, Z. Wang, and A. Loidl, Sub-gap optical response in the Kitaev spin-liquid candidate α-$RuCl_3$, J. Phys.: Condens. Matter **30**, 475604 (2018).

[30] E. Stavitski and F. M. de Groot, The CTM4XAS program for EELS and XAS spectral shape analysis of transition metal L edges, Micron **41**, 687 (2010).

[31] I. Pollini, Satellite structure in photoelectron spectra of $CrCl_3$, Solid State Commun. **113**, 559 (2000).

[32] A. Koitzsch, C. Habenicht, E. Müller, M. Knupfer, B. Büchner, H. C. Kandpal, J. van den Brink, D. Nowak, A. Isaeva, and

T. Doert, J_{eff} Description of the Honeycomb Mott Insulator α-$RuCl_3$, Phys. Rev. Lett. **117**, 126403 (2016).

[33] I. Pollini, Electron correlations and hybridization in chromium compounds, Solid State Commun. **106**, 549 (1998).

[34] I. Pollini and G. Spinolo, Intrinsic optical properties of $CrCl_3$, Phys. Status Solidi B **41**, 691 (1970).

[35] V. M. Bermudez and D. S. McClure, Spectroscopic studies of the two-dimensional magnetic insulators chromium trichloride and chromium tribromide—I, J. Phys. Chem. Solids **40**, 129 (1979).

[36] B. Carricabruru, J. Ferre, R. Mamy, I. Pollini, and J. Thomas, Optical and electron energy loss experiments in ionic $CrCl_3$ crystals, J. Phys. C **19**, 4985 (1986).

[37] L. J. Sandilands, Y. Tian, A. A. Reijnders, H.-S. Kim, K. W. Plumb, Y.-J. Kim, H.-Y. Kee, and K. S. Burch, Spin-orbit excitations and electronic structure of the putative Kitaev magnet $\alpha - RuCl_3$, Phys. Rev. B **93**, 075144 (2016).

[38] A. Koitzsch, E. Müller, M. Knupfer, B. Büchner, D. Nowak, A. Isaeva, T. Doert, M. Grüninger, S. Nishimoto, and J. van den Brink, Low-temperature enhancement of ferromagnetic Kitaev correlations in $\alpha - RuCl_3$, Phys. Rev. Materials **4**, 094408 (2020).

[39] J. Dillon, H. Kamimura, and J. Remeika, Magneto-optical properties of ferromagnetic chromium trihalides, J. Phys. Chem. Solids **27**, 1531 (1966).

[40] Y. Zhang, X. Wu, B. Lyu, M. Wu, S. Zhao, J. Chen, M. Jia, C. Zhang, L. Wang, X. Wang, Y. Chen, J. Mei, T. Taniguchi, K. Watanabe, H. Yan, Q. Liu, L. Huang, Y. Zhao, and M. Huang, Magnetic order-induced polarization anomaly of Raman scattering in 2d magnet CrI_3, Nano Lett. **20**, 729 (2020).

[41] M. McGuire, Crystal and magnetic structures in layered, transition metal dihalides and trihalides, Crystals **7**, 121 (2017).

[42] J. Fink, Recent developments in energy-loss spectroscopy, Adv. Electron. Electron Phys. **75**, 121 (1989).

[43] F. Roth, A. König, J. Fink, B. Büchner, and M. Knupfer, Electron energy-loss spectroscopy: A versatile tool for the investigations of plasmonic excitations, J. Electron Spectrosc. Relat. Phenom. **195**, 85 (2014).